



OPEN

Effects of waste oyster shell replacing fine aggregate on the dynamic mechanical characteristics of concrete

Yanling Lin^{1,2,3}, Yuzhe Ren^{2,3}, Tiange Ge^{2,3}, Mohammed Al-Ajamee^{4✉}, Yinglei Xu³, Abubaker Ahmed Mohamed Salih Mohamed⁴, Lu Ma⁵ & Hongxu Zhang¹

Waste oyster shells (WOS) have the potential to serve as a construction material, offering a sustainable alternative to traditional fine aggregates in the production of WOS concrete. This can play a critical role in reducing environmental issues resulting from the overexploitation of river sand and the haphazard disposal of WOS. Although existing research has predominantly focused on understanding the static mechanical characteristics of concrete when WOS is employed, the dynamic mechanical properties have still received less attention. To understand the impact of WOS as a substitute for fine aggregates on the dynamic mechanical properties of concrete, a series of tests employing Split Hopkinson Pressure Bar (SHPB) were carried out. The findings demonstrate that the peak stress and elastic modulus increase as the WOS substitution ratio (S_r) increases from 0 to 20% but exhibit an exponential decline as S_r increases from 20 to 100%. This response can be explained by the joint effects of the pore-filling effect caused by WOS sand and the increasing air content caused by WOS sand. As S_r increases from 0 to 20%, the pore-filling mechanism becomes predominant as the water absorption rate decreases slightly from 4.31 to 3.83%. However, for S_r increasing from 20 to 100%, the negative influence of the air content becomes the primary contributing factor, where the water absorption rate increases from 3.83 to 14.68%. Furthermore, under the same impact pressure, the concrete with $S_r = 20\%$ absorbed the most energy, providing the best dynamic mechanical performance. These findings highlight the potential use of WOS in concrete for improving its dynamic characteristics, promoting both sustainable construction and enhancing the material properties in impact-resistant structures.

Keywords Waste oyster shell, Fine aggregate, Dynamic mechanical behavior, Stress–strain relationship, Elastic modulus, Absorbed energy

With the increasing growth of the aquaculture industry, the issue of waste oyster shells (WOSs) has become a significant concern for many countries. Oyster shells make up between 37 and 70% of the total mass of oysters¹. It is estimated that approximately 3 million tons of WOS are generated annually in China². Improper disposal of these shells, due to residual flesh and microbial decomposition, can result in foul odor³, posing a threat to human health and causing environmental damage. While a small portion of WOS is currently reused for handicrafts, fertilizers^{4,5}, and food additives^{6,7}, a considerable quantity still requires urgent disposal.

One promising solution is the utilization of WOS in construction engineering, which serves as a substitute to mitigate the growing depletion of natural resources such as river sand, gravel, and cement ingredients. Recent studies have been conducted on incorporating WOS into various construction materials, including bricks⁸, cement additives⁹, mortar^{10–12}, and concrete^{13–15} by replacing a certain proportion of traditional ingredients with

¹School of Construction Engineering, Jiangsu Open University, No.399 North Jiangdong Road, Nanjing, China. ²Key Laboratory of Ministry of Education for Geomechanics and Embankment Engineering, Hohai University, No.1 Xikang Road, Nanjing, China. ³College of Civil and Transportation Engineering, Hohai University, No.1 Xikang Road, Nanjing, China. ⁴Department of Civil Engineering, Faculty of Engineering, University of Khartoum, Khartoum, Sudan. ⁵College of Architecture, Anhui Science and Technology University, No.1501, Huangshan Ave, Bengbu, China. ✉email: mohammedalajamee@gmail.com

WOS. These studies have demonstrated that WOS concrete is environmentally friendly and has the potential to be applied in coastal and offshore engineering projects^{14,15}.

Mechanical characteristics are essential for assessing the quality of concrete^{16,17}. A considerable amount of research has been carried out on the static mechanical behavior of concrete with WOS replacement. For instance, Yang et al.¹³ conducted compression tests by replacing 5–20% of the concrete fine aggregate with WOS, which has a particle size smaller than 5 mm. Their findings showed that the 28-day compressive strength of WOS-replaced concrete was greater than that of the control concrete specimens. Nonetheless, the elastic modulus decreased as the WOS replacement ratio (S_r) increased, given that the elastic modulus of WOS was lower than that of river sand. Similarly, Yang et al.¹⁸ further investigated on the long-term response of concrete with WOS-replaced fine aggregates. WOS S_r has a negligible effect on the compressive strength of 28-day, while after 28 days, the increase in compressive strength is expected and decreases with increasing S_r from 0 to 20%. Based on the studies of Refs.^{13,18}, Kuo et al.¹⁹ the same S_r used by Yang et al.¹³. However, with finer WOS particles (particle size less than 1.18 mm) 20% of the cement weight was replaced with fly ash. Their results were in line with these of Yang et al.¹³ reported that the compressive strength of the concrete with 5% S_r was greater than that of the control concrete. This phenomenon can be explained by the pore-filling effect of 5% WOS. However, the compressive strength decreased as the S_r increased, which was related to the absorption rate and porosity of WOS.

EO and Yi²⁰ replaced coarse and fine aggregates with WOS in volume ratios of 10–100% and 10–50%, respectively. The compression test results revealed that the compressive strength decreased as S_r increased, while the strength reduction rate decreased with increasing in water-cement ratio. Moreover, the WOS size also affects the strength. At the same S_r , concrete with coarse aggregates showed less compressive strength than concrete with fine aggregates. In terms of flexural tensile strength, concrete with 50% coarse/fine aggregate substitution exhibited a smaller reduction. Furthermore, relevant to these studies, Chen et al.²¹ conducted comparison tests between uneroded concrete and concrete with a fine aggregate S_r of 4–12% after 350 days of seawater erosion. It was found that concrete with S_r in the range of 8–10% offers the highest compressive strength and enhances the resistance against seawater erosion.

Consequently, previous studies have mostly concentrated on the static mechanical behavior of concrete with WOS, whereas the dynamic mechanical characteristics, which are vital indices for assessing the stability and reliability of revetment structure, remained unclear. Both drop-weight tests^{22,23} and Split Hopkinson Pressure Bar (SHPB) tests^{24,25} are commonly utilized to investigate the dynamic stress–strain behavior of concrete. Compared with drop-weight tests, SHPB tests have the advantages of producing high strain-rate loading and repeatable loading conditions. Therefore, in this study, SHPB tests were employed to explore the effects of WOS as a fine aggregate replacement on the dynamic mechanical characteristics of concrete.

Materials and methods

Material and specimen preparation

Figure 1a shows untreated WOS collected from the Yellow Sea, China. First, the shells were properly cleaned to remove any contaminants. Then, they were subjected to a drying process by placing them in an oven maintained at $95 \pm 2^\circ\text{C}$ for 24 h. Following the drying process, the shells were crushed and passed through a 3 mm sieve

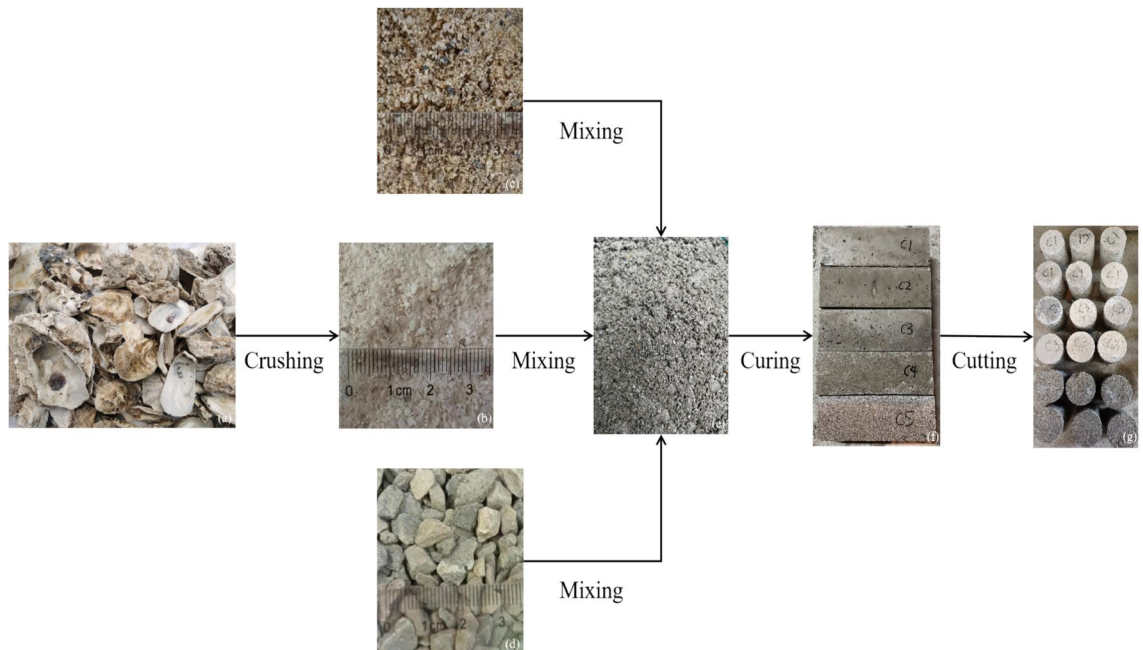


Fig. 1. Flowchart of WOS specimen preparation: (a) original WOS, (b) crushed WOS, (c) river sand, (d) gravel, (e) mixed aggregates, (f) concrete specimens, and (g) specimens for the SHPB tests.

to obtain WOS sand, which was utilized in place of fine aggregates in the concrete. The WOS sand exhibited a specific gravity of 2.25, as depicted in Fig. 1b. River sand, with a particle size less than 3 mm and a specific gravity of 2.63, was chosen as the concrete fine aggregate, as demonstrated in Fig. 1c. The concrete coarse aggregate, gravel, was obtained from Luhe, Nanjing, China, as shown in Fig. 1d, with a size range of 5 mm to 15 mm and a specific gravity of 2.48. The particle size distribution of the aggregates is displayed in Fig. 2, in which WOS sand is finer than river sand. SEM images of the fine aggregates are shown in Fig. 3. River sand generally exhibits a blocky appearance with concave and convex surfaces, which increases the grain roughness, whereas WOS sand

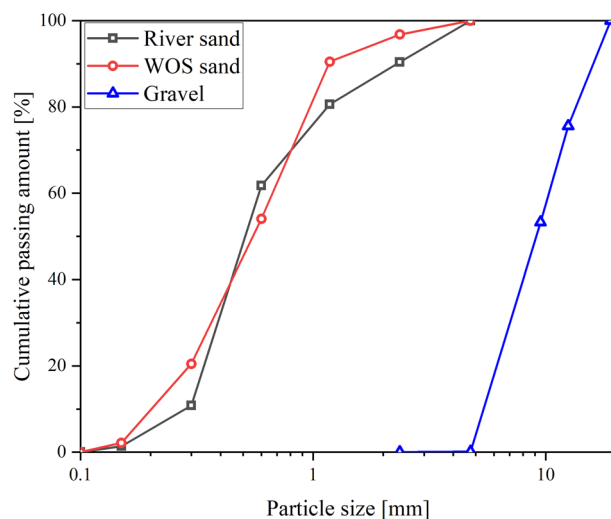


Fig. 2. Particle size distribution of aggregates.

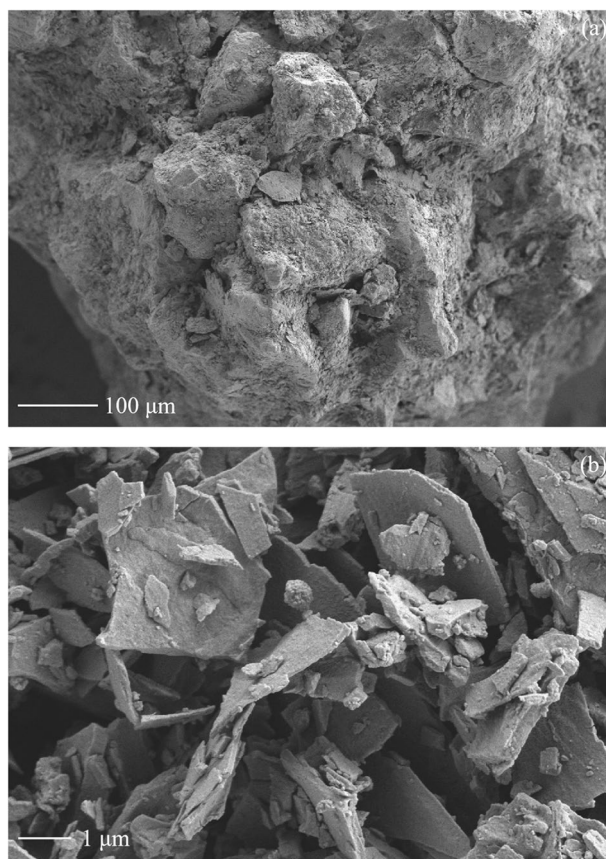


Fig. 3. SEM images of fine aggregates: (a) river sand, and (b) WOS sand.

appears as thin flakes with relatively smooth surfaces. The arrangement of WOS sand grains tends to form a porous structure, which is similar to the microstructure observed by Yoon et al.³. PO42.5 cement, manufactured by Conch China Cement Co., Ltd., served as the binding material for the concrete.

As shown in Table 1 and Fig. 1e, five WOS S_r samples were selected and the aggregates were mixed for the preparation of concrete specimens with a size of $100 \times 100 \times 300$ mm. Notably, no additional admixture was included in the mixture. Following a curing period of 3 days, the specimens were demolded and subsequently submerged in water at a temperature of 25 ± 1 °C for a total curing period of 28 days, thus replicating the coastal engineering application environment, (see Fig. 1f). Finally, cylindrical specimens, with a diameter of 74 mm and a height of 37 mm were cut from the aforementioned specimens to conduct subsequent SHPB tests, as shown in Fig. 1g.

Water absorption tests

For each type of concrete, three specimens with a size of $100 \times 100 \times 100$ mm at a curing age of 28 days were chosen for water absorption tests according to ASTM Standard C642-13²⁶. First, the concrete specimens were placed in an oven at 110 ± 2 °C for at least 24 h to dry. After that, the mass of the specimen was measured as M . Then, the concrete specimens were completely immersed in water for 2 days. After the surface moisture was removed with a towel, the mass of the surface-dried specimen was weighed as B . The absorption rate was calculated via Eq. (1):

$$W = \frac{B - M}{M} \times 100\%. \quad (1)$$

SHPB tests

Figure 4 illustrates the setup of the SHPB test equipment (type: LWKJ-HPKS-Y75, Luoyang Technology Co. Ltd., Luoyang, China) employed in this study. As shown in the figure the equipment consists of various components, including a gas gun, impact bar, incident bar, transmission bar, energy absorber and data processing system. To prevent premature specimen failure before the stress-equilibrium state due to the rapid increase in the incident pulse, a circular pulse shaper lubricated with vaseline was stuck on the impacted surface center of the incident bar. It has been proven that the material, diameter, and thickness of the pulse shaper influence the incident wave²⁷. Thus, after careful testing and optimization, circular pulse shapers manufactured of red copper with dimensions $\Phi 20$ mm \times 1.5 mm were fabricated. After vaseline lubrication, the concrete specimen was placed between the incident bar and transmission bar, while ensuring that the end surfaces of the bars remained parallel. Notably, both the incident and transmission bars had a cross-sectional diameter of 75 mm. Subsequently, when the gas gun propelled the impact bar toward the incident bar, the incident wave was generated. Once an incident wave arrives at the interface between the incident bar and specimen, a reflection occurs, resulting in the generation of the back wave. Similarly, transmitted waves were produced as the incident wave approached the contact between the specimen and transmission bar. The incident wave, back wave, and transmitted wave were recorded by resistance strain gauges affixed to the incident and transmission bars. The sampling rate was set at 500 kHz. Table 2 lists the experimental program, which involved selecting three different launching gas pressure levels. To ensure accuracy and minimize errors, three specimens were tested for each condition.

Based on the one-dimensional elastic wave theory, the stress, strain rate and strain of the specimen can be calculated from Eqs. (2)–(5), respectively.

$$\sigma = \frac{A_b E}{A_s} \varepsilon_t(t), \quad (2)$$

$$\dot{\varepsilon} = -\frac{2c_0}{l_0} \varepsilon_r(t), \quad (3)$$

$$\varepsilon = -\frac{2c_0}{l_0} \int_0^t \varepsilon_r(t) dt, \quad (4)$$

Type	w/c (by weight), %	F/A (by volume), %	WOS S_r (by volume), %	Unit weight, kg/m ³				
				w	c	S	G	WOS
C1	55	45	0	193	350	867.7	1000	0
C2			20	193	350	694.1	1000	148.5
C3			50	193	350	433.8	1000	371.2
C4			80	193	350	173.5	1000	593.8
C5			100	193	350	0	1000	742.3

Table 1. Design of mixture proportions. w water, c cement, F fine aggregate, A aggregate, S river sand, G gravel.

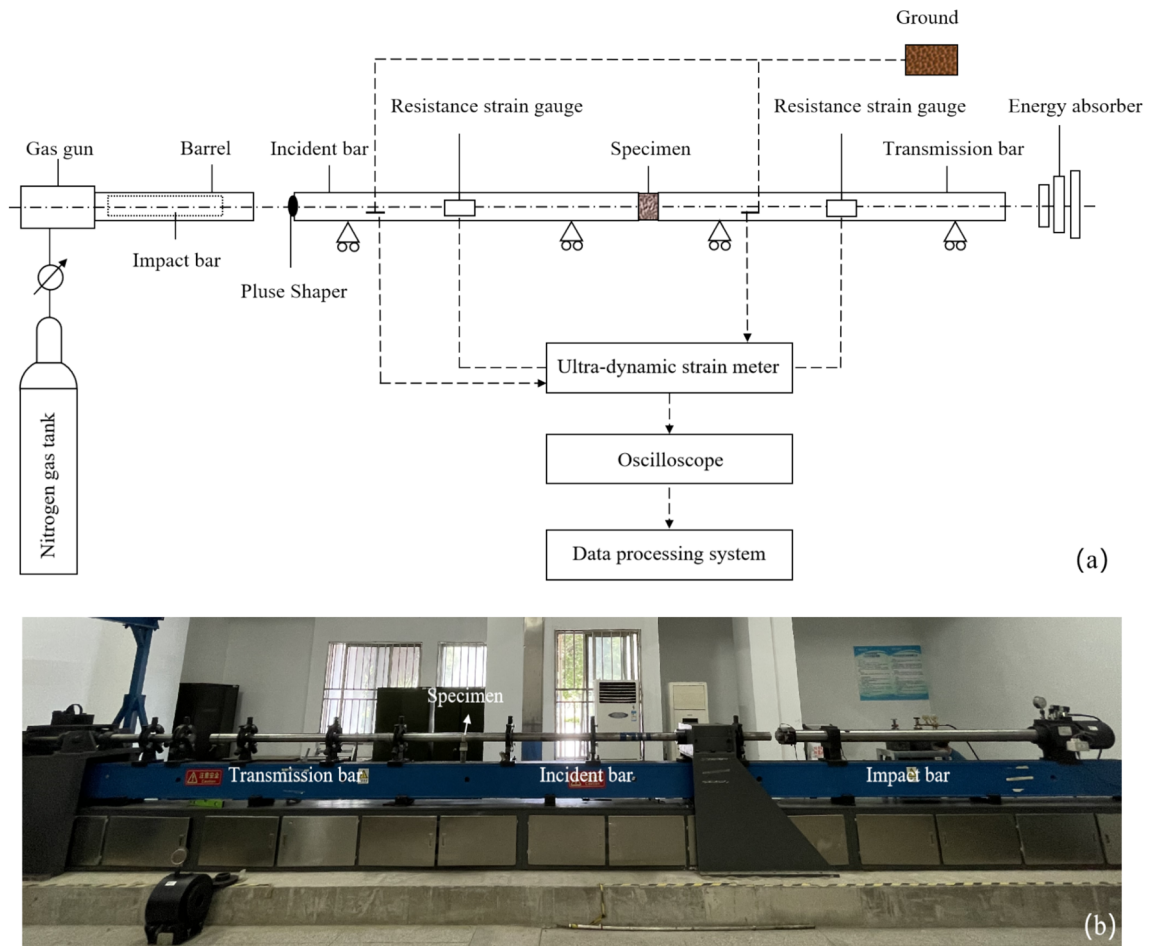


Fig. 4. SHPB test setup: (a) Schematic configuration, and (b) photograph.

Type	WOS substituted ratio (by volume), S_r [%]	Launching gas pressure, p [MPa]	Specimen quantity
C1	0	0.2	3
		0.3	3
		0.4	3
C2	20	0.2	3
		0.3	3
		0.4	3
C3	50	0.2	3
		0.3	3
		0.4	3
C4	80	0.2	3
		0.3	3
		0.4	3
C5	100	0.2	3
		0.3	3
		0.4	3

Table 2. Experimental programme.

$$c_0 = \sqrt{\frac{E}{\rho_0}}, \tag{5}$$

where $\epsilon_t(t)$ and $\epsilon_r(t)$ are the strains of the transmitted wave and back wave, respectively. A_b and A_s are the cross-sectional areas of the bars and specimen, respectively. E is the elastic modulus of bars, taken as 2.1×10^5 MPa,

while c_0 is the velocity of the elastic wave, obtained by Eq. (5). l_0 equals the height of the specimen. ρ_0 is the density of the bars, which is taken as 7820 kg/m^3 .

Result and discussion

Figure 5 displays the concrete specimens after the SHPB test under different launching gas pressure (p) levels. At a p of 0.2 MPa, even though the C1, C2, and C3 specimens experienced brittle failure, they did not completely shatter. In contrast, the C4 and C5 specimens showed more destruction, suggesting that increase in WOS S ,

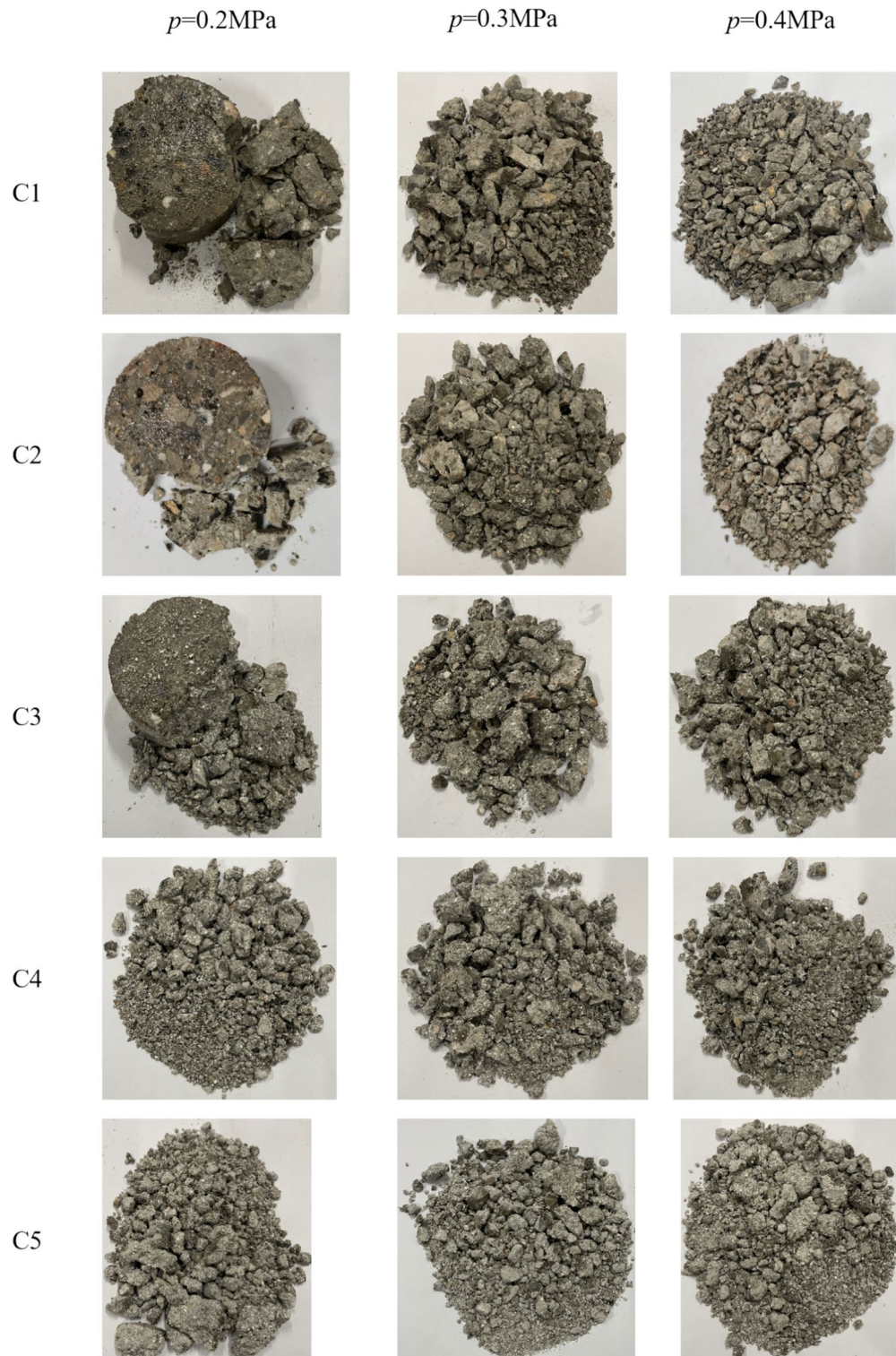


Fig. 5. Concrete specimens after SHPB tests under different launching gas pressure levels.

considerably reduced the impact resistance of the concrete specimens. This reflected the reduction in the bonding effect as the WOS S_r increased which may be because the flaky structure and smooth surface of the WOS sand reduced the bonding contact with the binding material. Furthermore, as p increased to 0.3 and 0.4 MPa, the concrete specimens were subjected to more comprehensive damage. This is because the increase in p signifies an increase in strain energy, while the energy absorption capability of concrete materials is limited. Thus, the release of additional energy is only facilitated through the expansion of cracks.

To obtain reliable and consistent results, the average of three specimens subjected to the same p for each type of concrete was considered. As shown in Fig. 6, the stress–strain relationship of the C1 specimens exhibited three distinct stages: the linear elastic stage, elastoplastic stage, and distortion stage. In the rising period of the stress–strain relationship, the curve first exhibited a rapid and linear increase, followed by a decrease in the rate of increase, accompanied by strain hardening. Once it reached the peak, the stress–strain curve began to decline, suggesting a softening of the strain, and resulting in total collapse of the specimen. Furthermore, as shown in Fig. 7, with increasing p , the slopes of the curves became steeper, indicating a greater degree of failure.

With a p of 0.2 MPa, increasing S_r from 0 to 20% resulted in an increase of approximately 9.5% in the peak stress (σ_p), from 46.5 to 50.9 MPa, as displayed in Fig. 7a. Correspondingly, for p values of 0.3 MPa and 0.4 MPa, σ_p increased from 50.3 and 60.2 to 58.5 MPa and 71.4 MPa, respectively. These increases correspond to enhancements of approximately 16.3% and 18.6%, as shown in Fig. 7b,c respectively. This observation clearly indicates that 20% S_r can effectively enhance the dynamic stress of ordinary concrete, which corresponds with the static mechanical characteristics of concrete with WOS replacement¹³. This may be due to two possible causes. First, the finer grading of WOS sand than that of river sand provides facilitates better filling of pores between aggregate grains, leading to increased compact density of the concrete. Second, the negative effect of the air content due to the porous structure of WOS is not significant. Although increased air content can make concrete more brittle, the change in air content resulting from 20% S_r replacement in fine aggregate is negligible, as observed by Yang et al.¹⁸. Figure 8 shows the results of the water absorption tests. The absorption rate decreases slightly from 4.31 to 3.83% as WOS S_r increases from 0 to 20%, which indicates that the concrete with 20% WOS S_r has fewer pores and a greater density. However, when S_r increased from 20 to 100%, the peak stress dramatically decreased at all p . When p is 0.2 MPa, 0.3 MPa, and 0.4 MPa, σ_p decreases sharply to 10.3 MPa, 20.0 MPa, and 28.6 MPa, representing reductions of 79.8%, 65.8%, and 60.0%, respectively. Moreover, the absorption rate increased sharply from 3.83 to 14.68%, indicating the increasing pore size. In this case, the dominant reason behind the strength loss is ascribed to the increased air content, which is in line with findings from static mechanical studies²⁰. On the one hand, the flaky structure of WOS sand gradually reduced the pore-filling effect during the further increase in WOS S_r , leading to more pores within the concrete. On the other hand, the pores in the WOS sand grains further result in more air. In addition, it is worth noting that with increasing p , the strain corresponding to σ_p (ε_{\max}) decreased. This is because as the rate of increase caused by p increases both the delayed elastic strain and the time interval for stress relaxation decrease²⁸.

The connections between σ_p and WOS S_r are illustrated in Fig. 9. The σ_p first increases with increasing S_r , but then the trend is inverted, and the peak stress starts to decrease exponentially as S_r exceeds 20%. However, the rate of reduction gradually decreased as S_r increased, indicating a diminishing effect of the WOS air content on σ_p .

Furthermore, the elastic modulus, E_0 , is taken from the slope of the secant line connecting 10% and 40% of the σ_p ²⁹, written using Eq. (6):

$$E_0 = \frac{\sigma_{40} - \sigma_{10}}{\varepsilon_{40} - \varepsilon_{10}}, \quad (6)$$

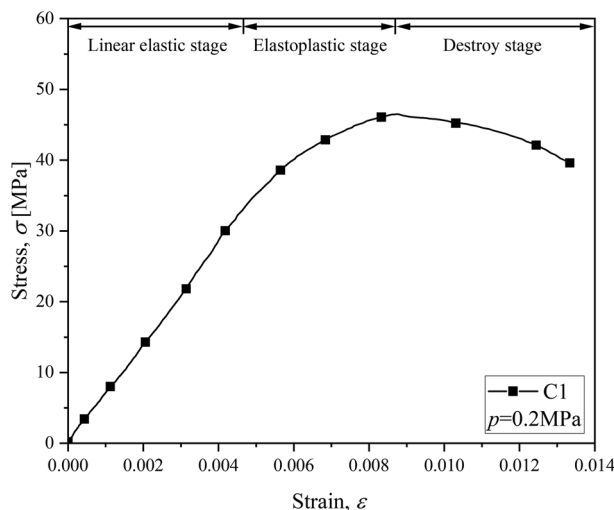


Fig. 6. Three stages of the dynamic stress–strain curves of the concrete specimens.

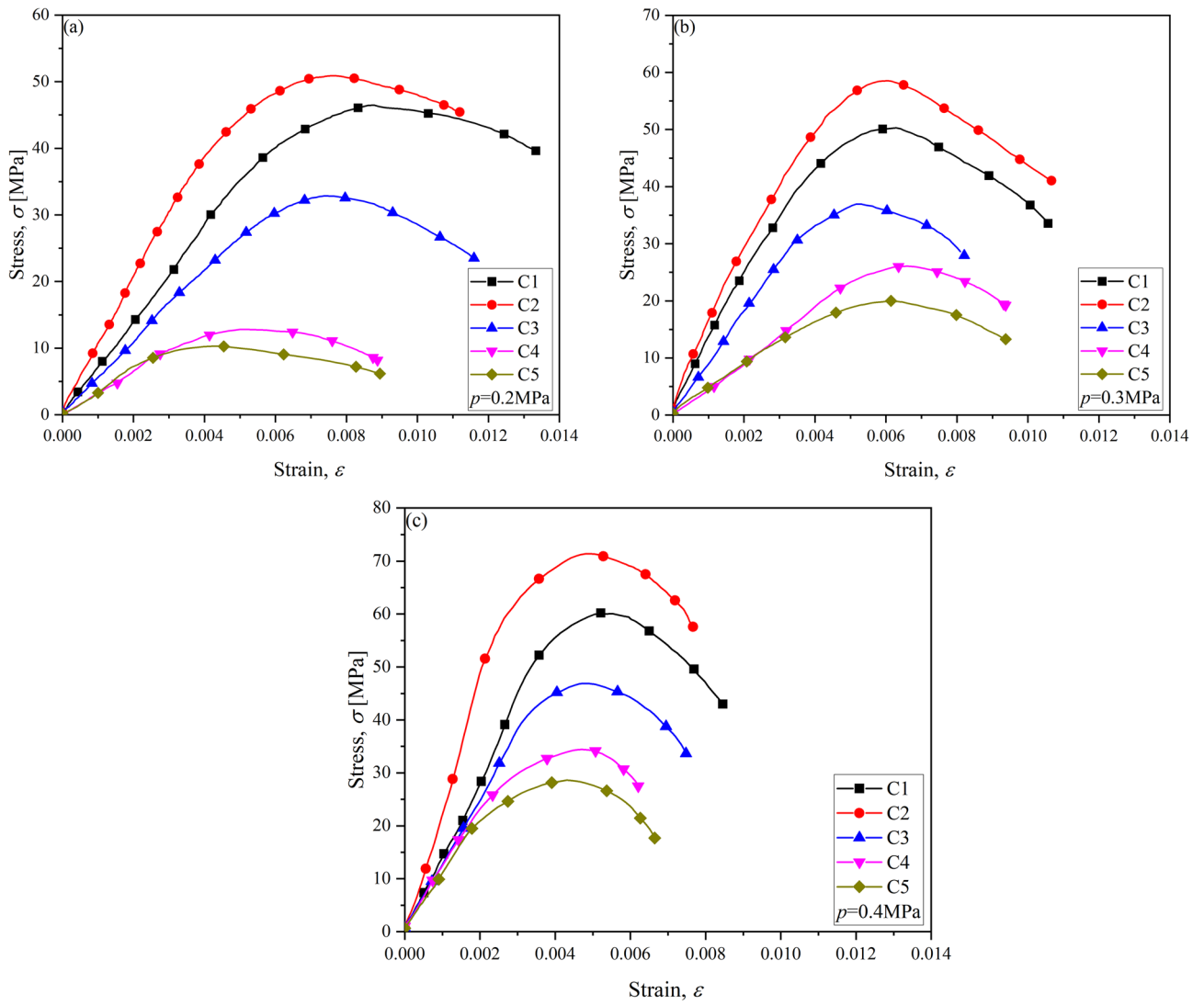


Fig. 7. Dynamic stress–strain relationship of the concrete specimens with WOS fine aggregate replacement: (a) $p=0.2$ MPa, (b) $p=0.3$ MPa, and (c) $p=0.4$ MPa.

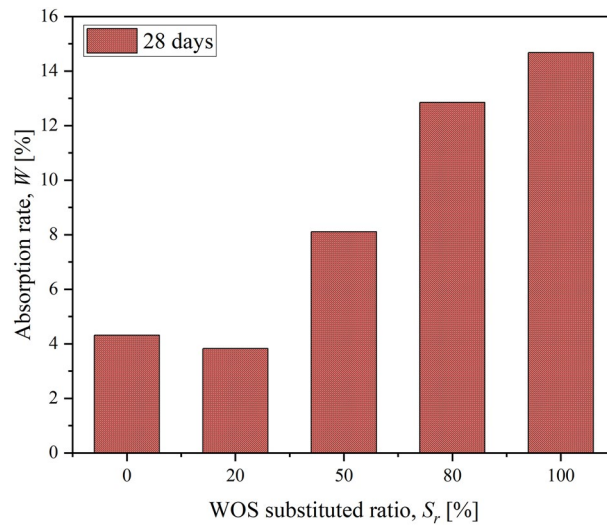


Fig. 8. Absorption rate of concrete with different WOS substitution ratios.

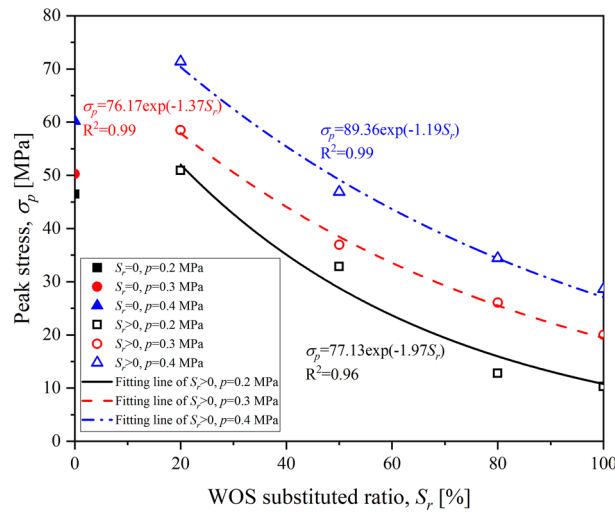


Fig. 9. Relationship between the peak stress and WOS substituted ratio.

where σ_{40} and σ_{10} are 40% and 10% of the σ_p , respectively, whereas ε_{40} and ε_{10} are the strains corresponding to σ_{40} and σ_{10} , respectively. Figure 10 depicts the relationship between E_0 and WOS S_r . Similar to the relationship between σ_p and WOS S_r , when S_r increased from 0 to 20%, the E_0 values increased from 6.7 GPa, 12.3 GPa, and 13.5 GPa to 10.1 GPa, 14.0 GPa, and 23.3 GPa under p values of 0.2 MPa, 0.3 MPa, and 0.4 MPa, respectively. However, this result contradicts the observations about the static mechanical behavior observed by Yang et al.¹³, which may be due to the pore-filling effect. However, when S_r increased from 20 to 100%, E_0 decreased from 10.1 GPa, 14.0 GPa, and 23.3 GPa to 3.7 GPa, 4.1 GPa, and 10.5 GPa under p value of 0.2 MPa, 0.3 MPa, and 0.4 MPa, respectively. The reduction initially occurred followed by sharp a decrease, exhibiting an exponential pattern similar to that of σ_p . As previously analyzed, this may be because the porous structure of WOS sand led to an increase in brittleness which resulted in a lower elastic modulus than that of river sand. Furthermore, the smooth surface of WOS sand may weaken the bonding effect between the aggregates and the binding material, resulting in a lower elastic modulus, as the concrete becomes more susceptible to cracking under dynamic impact.

Figure 11 displays the evolution of the absorbed energy with strain during the SHPB tests. The absorbed energy, E_a , is calculated by Eqs. (7) and (8):

$$E_a = V \cdot \int_{\varepsilon=0}^{\varepsilon=\varepsilon_{\max}} \sigma \cdot \varepsilon d\varepsilon, \tag{7}$$

$$V = \pi r^2 l_0, \tag{8}$$

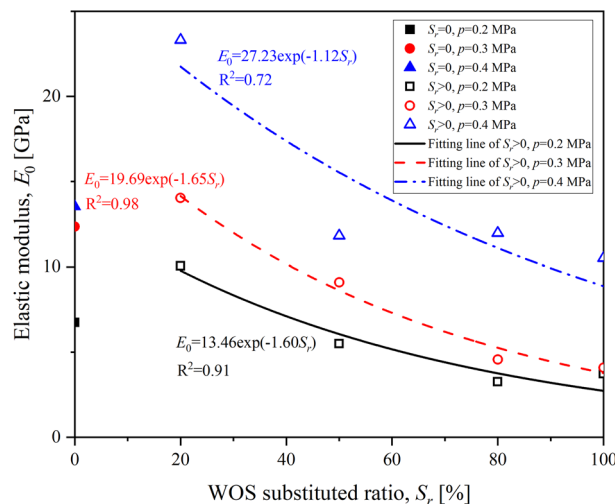


Fig. 10. Relationship between the elastic modulus and WOS substitution ratios.

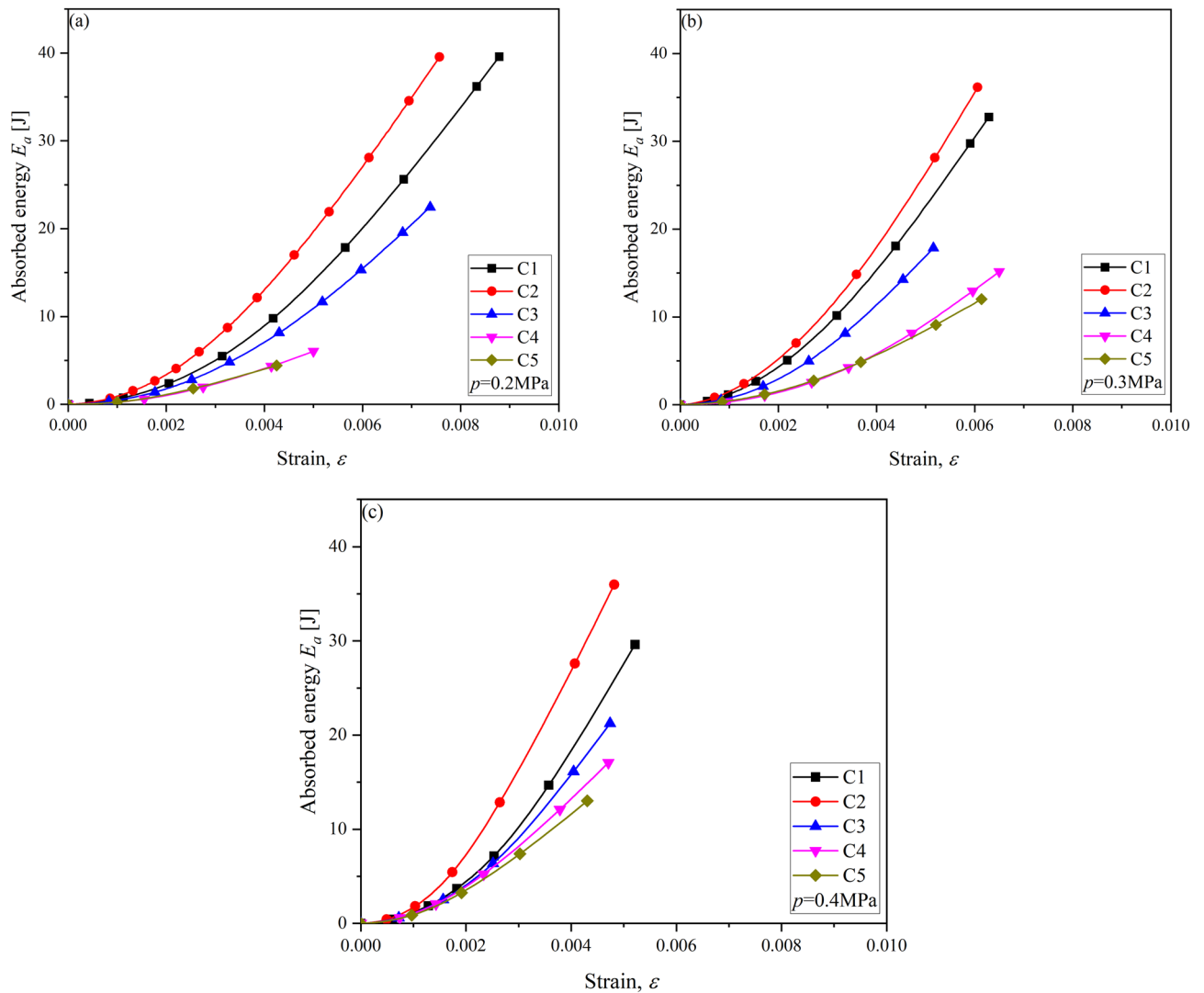


Fig. 11. Evolution of the absorbed energy with strain during the SHPB tests: (a) $p=0.2$ MPa, (b) $p=0.3$ MPa, and (c) $p=0.4$ MPa.

where V is the volume of the concrete specimen and σ and ϵ are the stress and strain of the concrete specimen during the SHPB tests, respectively. r and l_0 are the radius and height of the concrete specimens, taken as 37 mm and 37 mm, respectively. σ_p increased with increasing ϵ until the concrete specimens were destroyed. When S_r increased from 0 to 20%, E_a remained at approximately 39 J under p of 0.2 MPa, but increased from 32.7 J and 29.6 J to 36.1 and 35.9 J, respectively, when p was of 0.3 MPa and 0.4 MPa, respectively. This proves that 20% S_r WOS concrete can absorb more energy than plain concrete before failure. However, when S_r increased from 20 to 100%, E_a decreased sharply from 39.5 J, 36.1 J and 35.9 J to 4.4 J, 12.0 J and 13.0 J under p value of 0.2 MPa, 0.3 MPa, and 0.4 MPa, respectively, which demonstrated that the concrete specimens with WOS S_r contents greater than 20% had less impact resistance.

From Fig. 7a–c, it can be observed that the strain related to the σ_p decreased with increasing S_r , which suggests that WOS aggregate concrete exhibits lower ductility than ordinary concrete. This finding contradicts the results of a drop-weight test study by Liu et al.²², which concluded that a small and uniform pore structure could contribute to the resistance to impact. There are two possible explanations for this discrepancy. First, the impact resistance of the pore structure may vary at different strain rates. In drop-weight experiments, the strain rate typically ranges from 10^{-3} to 10^1 s $^{-1}$, while in SHPB tests, it falls in the range of 10^1 to 10^3 s $^{-1}$.²⁵ The impact resistance of the pore structure may be effective at lower strain rates but may exhibit a limited effect at higher strain rates. Second, the number of pores may also affect the impact resistance. The air content in WOS aggregates¹⁸, may be much lower than that in foam concrete investigated in the work of Liu et al.²².

Conclusion

WOS aggregates have the potential to be widely used in construction engineering. While numerous investigations have been performed on the static mechanical behavior of concrete with WOS substitution, particularly its compressive strength and elastic modulus, there is limited research on its dynamic mechanical behavior. Therefore, in

this study, a number of SHPB tests were carried out to research the effects of WOS replacement on the dynamic mechanical characteristics of concrete. The following conclusions can be drawn in light of the results obtained:

- Increasing S_r from 0 to 20% results increases in σ_p and E_0 , primarily due to the pore-filling effect. E_a remained almost constant at 0.2 MPa launching gas pressure but increased from 32.7 and 29.6 to 36.1 and 35.9 J, respectively, when p was of 0.3 MPa and 0.4 MPa, respectively.
- Under p value of 0.2 MPa, 0.3 MPa, and 0.4 MPa σ_p increased by approximately 9.5%, 16.3%, and 18.6%, respectively. The E_0 values increased from 6.7, 12.3 and 13.5 to 10.1 GPa, 14.0 GPa, and 23.3 GPa respectively.
- When S_r increased from 20 to 100%, σ_p and E_0 decreased exponentially, which was mainly controlled by the negative effect of the air content. E_a decreased from 39.5 J, 36.1 J and 35.9 J to 4.4 J, 12.0 J and 13.0 J when p was 0.2 MPa, 0.3 MPa, and 0.4 MPa, respectively.
- At p value of 0.2 MPa, 0.3 MPa, and 0.4 MPa, σ_p decreases sharply to 10.3 MPa, 20.0 MPa, and 28.6 MPa, representing reductions of 79.8%, 65.8%, and 60.0%, respectively. However, E_0 decreased from 10.1 GPa, 14.0 GPa, and 23.3 GPa to 3.7 GPa, 4.1 GPa, and 10.5 GPa respectively.

The findings, thus, suggested that σ_p and E_0 increased with increasing WOS S_r . However, exact relationships could not be established in the study due to the limited data and the range of S_r considered in this study. Future studies will focus on further refining the S_r range and exploring the use of additives to improve the dynamic characteristics of concrete.

Data availability

The datasets used and/or analysed during the current study available from the corresponding author on reasonable request.

Received: 30 March 2024; Accepted: 18 August 2024

Published online: 27 August 2024

References

1. Yao, Z. *et al.* Bivalve shell: Not an abundant useless waste but a functional and versatile biomaterial. *Crit. Rev. Environ. Sci. Technol.* **44**(22), 2502–2530 (2014).
2. Li, G., Xu, X., Chen, E., Fan, J. & Xiong, G. Properties of cement-based bricks with oyster-shells ash. *J. Clean. Prod.* **91**, 279–287 (2015).
3. Yoon, G.-L., Kim, B.-T., Kim, B.-O. & Han, S.-H. Chemical–mechanical characteristics of crushed oyster-shell. *Waste Manag.* **23**(9), 825–834 (2003).
4. Lee, C. H., Lee, D. K., Ali, M. A. & Kim, P. J. Effects of oyster shell on soil chemical and biological properties and cabbage productivity as a liming materials. *Waste Manag.* **28**(12), 2702–2708 (2008).
5. Kwon, Y. T., Lee, C. W. & Yun, J. H. Development of vermicast from sludge and powdered oyster shell. *J. Clean. Prod.* **17**(7), 708–711 (2009).
6. Choi, Y. M., Whang, J. H., Kim, J. M. & Suh, H. J. The effect of oyster shell powder on the extension of the shelf-life of Kimchi. *Food Control* **17**(9), 695–699 (2006).
7. Kim, Y. S., Choi, Y. M., Noh, D. O., Cho, S. Y. & Suh, H. J. The effect of oyster shell powder on the extension of the shelf life of tofu. *Food Chem.* **103**(1), 155–160 (2007).
8. Chiou, I. J., Chen, C. H. & Li, Y. H. Using oyster-shell foamed bricks to neutralize the acidity of recycled rainwater. *Constr. Build. Mater.* **64**, 480–487 (2014).
9. Seo, J. H., Park, S. M., Yang, B. J. & Jang, J. G. Calcined oyster shell powder as an expansive additive in cement mortar. *Materials* **12**(8), 1322 (2019).
10. Liu, R., Chen, D., Cai, X., Deng, Z. & Liao, Y. Hardened properties of mortar mixtures containing pre-treated waste oyster shells. *J. Clean. Prod.* **266**, 121729 (2020).
11. Liao, Y., Wang, X., Kong, D., Da, B. & Chen, D. Experiment research on effect of oyster shell particle size on mortar transmission properties. *Constr. Build. Mater.* **375**, 131012 (2023).
12. Song, Q. *et al.* Properties of water-repellent concrete mortar containing superhydrophobic oyster shell powder. *Constr. Build. Mater.* **337**, 127423 (2022).
13. Yang, E.-I., Yi, S.-T. & Leem, Y.-M. Effect of oyster shell substituted for fine aggregate on concrete characteristics: Part I. Fundamental properties. *Cem. Concr. Res.* **35**(11), 2175–2182 (2005).
14. Uddin, M. J., Smith, K. J. & Hargis, C. W. Development of pervious oyster shell habitat (POSH) concrete for reef restoration and living shorelines. *Constr. Build. Mater.* **295**, 123685 (2021).
15. Kong, J. *et al.* Recycling of waste oyster shell and recycled aggregate in the porous ecological concrete used for artificial reefs. *Constr. Build. Mater.* **323**, 126447 (2022).
16. Abbara, A. A. *et al.* Uniaxial compressive stress–strain relationship for rubberized concrete with coarse aggregate replacement up to 100%. *Case Stud. Constr. Mater.* **17**, e01336 (2022).
17. Adhikary, S. K. *et al.* Lightweight self-compacting concrete: A review. *Resour. Conserv. Recycl. Adv.* **15**, 200107 (2022).
18. Yang, E.-I., Kim, M.-Y., Park, H.-G. & Yi, S.-T. Effect of partial replacement of sand with dry oyster shell on the long-term performance of concrete. *Constr. Build. Mater.* **24**(5), 758–765 (2010).
19. Kuo, W.-T., Wang, H.-Y., Shu, C.-Y. & Su, D.-S. Engineering properties of controlled low-strength materials containing waste oyster shells. *Constr. Build. Mater.* **46**, 128–133 (2013).
20. Eo, S.-H. & Yi, S.-T. Effect of oyster shell as an aggregate replacement on the characteristics of concrete. *Mag. Concr. Res.* **67**(15), 833–842 (2015).
21. Hai-Yan, C. *et al.* Effects of crushed oyster shell on strength and durability of marine concrete containing fly ash and blastfurnace slag. *Mater. Sci.* **25**(1), 97–107 (2019).
22. Liu, J., Ren, Y., Chen, R., Wu, Y. & Lei, W. The effect of pore structure on impact behavior of concrete hollow brick, autoclaved aerated concrete and foamed concrete. *Materials* **15**(12), 4075 (2022).
23. Zhang, W., Chen, S. & Liu, Y. Effect of weight and drop height of hammer on the flexural impact performance of fiber-reinforced concrete. *Constr. Build. Mater.* **140**, 31–35 (2017).
24. Ren, L. *et al.* Evaluation of typical dynamic damage models used for UHPC based on SHPB technology. *Eng. Fract. Mech.* **269**, 108562 (2022).

25. Yu, Q., Zhuang, W. & Shi, C. Research progress on the dynamic compressive properties of ultra-high performance concrete under high strain rates. *Cem. Concr. Compos.* **124**, 104258 (2021).
26. ASTM-C642-13. *Standard Test Method for Density, Absorption, and Voids in Harden Concrete* (ASTM, 2013).
27. Wang, J., Li, W., Xu, L., Du, Z. & Gao, G. Experimental study on pulse shaping techniques of large diameter SHPB apparatus for concrete. *Lat. Am. J. Solids Struct.* **18**, e343 (2021).
28. Bischoff, P. H. & Perry, S. H. Compressive behaviour of concrete at high strain rates. *Mater. Struct.* **24**, 425–450 (1991).
29. Fu, Q. *et al.* Impact characterization and modelling of cement and asphalt mortar based on SHPB experiments. *Int. J. Impact Eng.* **106**, 44–52 (2017).

Author contributions

Y L: Conceptualization, Methodology, Investigation, Validation, Writing-original draft. Y R: Conceptualization, Methodology, Investigation, Data curation, Writing-original draft. Tiange Ge: Investigation, Validation, Data curation. M A: Investigation, Validation, Writing-review & editing. Y X: Investigation, Writing-review & editing. A A M S M: Validation, Writing-review & editing. L M: Resources, Writing-review & editing. H Z: Investigation.

Competing interests

The authors declare no competing interests.

Additional information

Correspondence and requests for materials should be addressed to M.A.-A.

Reprints and permissions information is available at www.nature.com/reprints.

Publisher's note Springer Nature remains neutral with regard to jurisdictional claims in published maps and institutional affiliations.

Open Access This article is licensed under a Creative Commons Attribution-NonCommercial-NoDerivatives 4.0 International License, which permits any non-commercial use, sharing, distribution and reproduction in any medium or format, as long as you give appropriate credit to the original author(s) and the source, provide a link to the Creative Commons licence, and indicate if you modified the licensed material. You do not have permission under this licence to share adapted material derived from this article or parts of it. The images or other third party material in this article are included in the article's Creative Commons licence, unless indicated otherwise in a credit line to the material. If material is not included in the article's Creative Commons licence and your intended use is not permitted by statutory regulation or exceeds the permitted use, you will need to obtain permission directly from the copyright holder. To view a copy of this licence, visit <http://creativecommons.org/licenses/by-nc-nd/4.0/>.

© The Author(s) 2024